ELSEVIER

Surface Science 501 (2002) 155–167

SURFACE SCIENCE

www.elsevier.com/locate/susc

Scanning tunneling microscopy and spectroscopy study on the submonolayer growth of Mn on Fe(0 0 1)

M.M.J. Bischoff, T. Yamada, A.J. Quinn [1], H. van Kempen *

Research Institute for Materials, University of Nijmegen, Toernooiveld 1, 6525 ED Nijmegen, Netherlands

Received 12 October 2001; accepted for publication 7 December 2001

Abstract

The submonolayer growth of Mn on Fe(0 0 1) in the temperature range between 50 and 200 °C is studied by scanning tunneling microscopy and scanning tunneling spectroscopy. For growth temperatures above 100 °C, atomically resolved STM images with chemical contrast clearly reveal the incorporation of Mn atoms in the Fe(0 0 1) substrate. The fraction of place exchanged Mn atoms is observed to increase with growth temperature. Although on islands a c(2×2) structure forms locally which is attributed to an ordered MnFe surface alloy, long range order could not be obtained for the growth temperatures and coverages studied. Spectroscopy results are presented for clean Fe(0 0 1), pure Mn adislands, single incorporated Mn atoms and c(2×2)-ordered MnFe areas. In contrast to embedded Cr atoms in the Fe(0 0 1) surface [Phys. Rev. Lett. 76 (1996) 4175], isolated embedded Mn atoms do not lead to double peak structures in $\mathrm{d}I/\mathrm{d}V$ curves. Nevertheless, on the ordered c(2×2) MnFe structure and the pure Mn monoatomic islands surface states are detected as peaks in the $\mathrm{d}I/\mathrm{d}V$ and $(\mathrm{d}I/\mathrm{d}V)/(I/V)$ curves. However, due to the strong influence of a tip-dependent background on these peaks, the corresponding surface state energies cannot be found directly from those curves. The real surface state energies were recovered by normalizing the measured $\mathrm{d}I/\mathrm{d}V$ curves by fitted quadratic backgrounds. Thus, surface state energies of about +0.35 and +0.25 eV are estimated for pure Mn islands and alloyed MnFe areas, respectively.

Keywords: Epitaxy; Iron; Manganese; Scanning tunneling microscopy; Scanning tunneling spectroscopies; Surface electronic phenomena (work function, surface potential, surface states, etc.); Surface structure, morphology, roughness, and topography; Whiskers

1. Introduction

During the last decade a large number of experimental and theoretical studies have been dedicated to elucidating the interrelation between structure and magnetic/electronic properties of transition metals. Molecular-beam-epitaxial techniques allow growth of low-dimensional and strained metal structures often with novel magnetic and electronic properties. A classic example

* Corresponding author. Tel.: +31-24-3653499; fax: +31-24-3652190.

E-mail address: hvk@sci.kun.nl (H. van Kempen).

[1] Present address: National Microelectronics Research Centre, University College, Cork, Ireland.

0039-6028/02/$ - see front matter
PII: S0039-6028(01)01946-X

of a system where structure, magnetism, and electronic effects are interwoven in a complex fashion is Mn/Fe(0 0 1) [1–22].

For Mn films thicker than 3–5 monolayers (ML), both theoretical and experimental studies confirm the layered antiferromagnetism of the Mn layers (see e.g. [1,2] and references therein). The Mn film grows in a distorted bcc structure with the in-plane lattice constant equal to the Fe(0 0 1) bulk lattice constant of 0.287 nm but with the out-of-plane lattice constant expanded to 0.323 nm, i.e. body-centered-tetragonal [3,4]. Layer-by-layer growth is followed by a transition to three-dimensional growth depending on growth temperature and substrate quality [1,2,5,6]. Between 10 and 17 ML a $c(4 \times 4)$ superstructure was reported by Andrieu et al. [6]. Finally, thick Mn films (above 17 ML in [6]) relax in the Mnα structure which is the stable bulk phase of Mn at room temperature (its cubic unit cell includes 58 atoms).

In the ultrathin limit, however, conflicting results have been reported in both theoretical and experimental studies. Andrieu et al. showed by X-ray magnetic circular dichroism experiments that in the submonolayer regime the Mn atoms couple ferromagnetically to each other and couple ferromagnetically to the substrate [6,7]. They also showed quite convincingly that oxygen contamination changes the coupling to the substrate to antiferromagnetic [8] which could explain the conflicting experimental results of other groups [9–11]. Furthermore, extended X-ray absorption spectroscopy (EXAFS) showed that the first monolayer grows with an interlayer distance of 0.148 nm [6]. However, these experiments focussed on room temperature grown Mn films.

Recent ab initio calculations showed that the $c(2 \times 2)$ antiferrimagnetic configuration and the $p(2 \times 2)$ ferromagnetic configuration (i.e. three Mn atoms ferromagnetically coupled and one antiferromagnetically) are nearly degenerate [12–16]. Calculations for a bilayer surface-ordered MnFe alloy with $c(2 \times 2)$ arrangement showed that this mixed configuration is as stable as the ground states of the pure Mn configurations [16]. Calculations for the dilute limit of 3d atoms on the Fe(0 0 1) surface by Nonas et al. showed that Mn atoms (and in fact all 3d transition metals except Co) have a tendency to place exchange with Fe substrate atoms [17]. For Cr impurities these results were in perfect agreement with the scanning tunneling microscopy (STM) and spectroscopy (STS) study of Davies et al. [18,19] and even the experimentally observed repulsion of surface nearest and next-nearest Cr neighbors could be reproduced in the calculations. In contrast to Cr impurities, for Mn only a strong repulsion on surface nearest neighbors was predicted whose origin was found to be frustration: the surface nearest-neighbor Mn atoms favor antiferromagnetic coupling with each other but this is hindered by the strong antiferromagnetic coupling with the substrate Fe atoms. The embedded 3d atoms in the Fe(0 0 1) surface were theoretically found to give rise to characteristic double peak structures in the vacuum local density of states (LDOS) around the Fermi level [20] and therefore chemical identification as was shown for Cr on Fe(0 0 1) [18] might also be possible for these elements. However, compared to the Fe(0 0 1)-derived surface state peak which is always present, the additional 3d-impurity peak is predicted to be strongest for the elements at the beginning of the 3d-series (i.e. V and Cr) and weakest for Mn [20].

The interfacial alloying of the Mn/Fe(0 0 1) system was experimentally verified by extremely surface sensitive proton-induced Auger electron spectroscopy measurements: Igel et al. found that for growth around 300 °C only 40% of the deposited monolayer Mn atoms could still be found on top of the surface layer implying that 60% of the deposited Mn atoms underwent place exchanges with the substrate Fe atoms [21]. Increased intermixing for a two monolayer Mn film on Fe(0 0 1) was also reported by Walker and Hopster after annealing above 150 °C [22].

In this paper, we report on an STM and STS study on the growth of submonolayer Mn films on Fe(0 0 1) whiskers in the temperature range between 50 and 200 °C. Atomically and chemically resolved STM imaging allow us to study the intermixing behavior of Mn atoms in the Fe(0 0 1) surface as a function of growth temperature. Motivated by the chemical identification achieved by STS for the Cr/Fe(0 0 1) system [18,19], STS measurements will be presented for all structures

observed. For the first time, the influence of a tip dependent background on the apparent peak energies in dI/dV and $(dI/dV)/(I/V)$ curves is discussed in the context of real experiments.

2. Experimental

The experiments were performed under ultra-high vacuum conditions (base pressure less than 5×11^{-11} mbar). Single crystal Fe(0 0 1) whiskers with typical sizes of $7 \times 1 \times 1$ mm^3 grown at Simon Fraser University (Burnaby, Canada) were used as substrate material [23]. The whiskers were cleaned by repetitive cycles of Ar ion sputtering (750 eV) around 750 °C. In the final cleaning step, long post-anneals after sputtering were avoided. The concentration of impurities (mainly oxygen) was typically below 0.01 ML as estimated by Auger electron spectroscopy and atomically resolved STM images. Furthermore, this treatment is sufficient to heal the sputter damage and terraces with widths up to 400 nm are generally observed. Mn was sublimated from a Knudsen cell at a rate of 0.2 ML/min as measured by a quartz crystal microbalance. In this work, 1 ML is defined as a complete overlayer with Fe(0 0 1) bulk lattice constant (1.214×10^{15} atoms cm^{-2}). By proper shielding of this cell with a liquid nitrogen cooled baffle and comprehensive degassing, the pressure was maintained below 3×10^{-10} mbar during growth. The sample was annealed using a resistive heater which limited the maximum growth temperature to around 200 °C. Temperature measurements were performed by a thermocouple which was not in direct contact with the sample. Therefore, the estimated error in the temperature measurements is relatively high: ±30 °C at 200 °C.

After growth the sample was transported as quickly as possible to the room temperature STM (Omicron UHV STM-1) in the analysis chamber. In this small chamber the background CO pressure is estimated to be 4×10^{-12} mbar from residual gas analysis by mass spectrometry. This low CO partial pressure is quite important considering the fast dissociation of CO on Mn films as discussed by Andrieu et al. [8]. Electrochemically etched W tips were used which were cleaned and sharpened in situ by Ne self-sputtering [24]. Field emission spectroscopy confirmed the sharpness of the tips (radii less than 10 nm). STS measurements were performed by recording $I(V)$ curves under open feedback conditions. To minimize the influence of the drift (~0.3 nm/min shortly after sample preparation), these $I(V)$ curves were recorded as quickly as possible (typically 52 ms for a 100 point curve). The drift is mainly caused by contraction (after heating) of the whisker along its long axis relative to the Ta sample holder. The relatively large distance (~5 mm) between tip position and the point where the whisker is fixed to the holder is not favorable in this perspective. To be able to compare topographic features with spectroscopic ones, $I(V)$ curves were measured simultaneously with conventional constant current images but at a reduced resolution of typically 75 points × 75 lines to avoid strong distortions due to drift. The $I(V)$ curves were numerically differentiated using a 5-point window to obtain dI/dV.

3. Results and discussion

3.1. Submonolayer growth at low temperature: pure Mn islands

An STM image of the Fe(0 0 1) surface after deposition of 0.2 ML (quartz crystal calibration) Mn at a substrate temperature of 50 °C is shown in Fig. 1a. The island coverage is estimated to be 0.17 ML from histogram analysis. However, the ragged step edge in Fig. 1a shows that small Mn islands nucleated at the step edge. These islands can easily be missed in a histogram analysis and therefore, coverages were determined on large terraces (>200 × 200 nm^2) where the influence of Fe(0 0 1) steps can be neglected. The histogram analysis also shows that the height of the Mn islands is slightly higher (0.156 ± 0.005 nm) than the Fe(0 0 1) step height (0.144 ± 0.005 nm). To avoid electronic effects, step heights were measured at large negative bias voltages where the STS results did not reveal any features (see below). Furthermore, apparent barrier height measurements were performed which showed that the effect of different local work functions on the apparent step heights can be

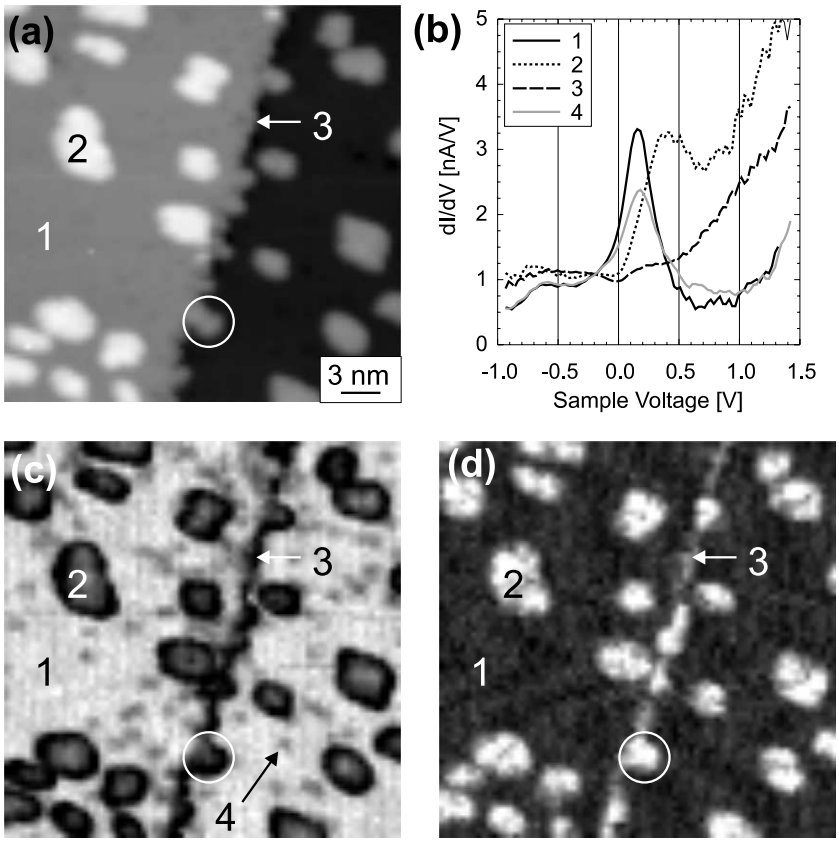

Fig. 1. (a) Constant current STM image of 0.2 ML Mn deposited on Fe(0 0 1) at 50 °C (tunneling current $I = 0.5$ nA, sample voltage $V_s = -0.5$ V, scan size is 30×30 nm^2) showing monolayer high islands (0.156 nm high). The white circle marks a small Mn island which nucleated at the step edge. A dI/dV curve is obtained at each pixel (75×75) of this image. (b) Averaged dI/dV curves representative of four different features in (a). Curve 1 is measured at the Fe(0 0 1) terrace, curve 2 at the islands, curve 3 at the steps, and curve 4 at the oxygen impurities. Numbers refer to numbers in (a), (c) and (d). (c) and (d) show dI/dV maps at $V_s = +0.16$ and $+0.99$ V, respectively.

excluded [25]. Therefore, these step heights are believed to reflect the real interlayer spacings.

A dI/dV curve was measured at every pixel of Fig. 1a. Four different types of dI/dV curves can be distinguished and averages of these curves (typically obtained from 10 single curves) are shown in Fig. 1b. Curve 1 is the average of the dI/dV curves measured on the Fe(0 0 1) terrace. It shows a strong peak at +0.16 V which is attributed to a localized minority spin band surface state of d_{z^2} symmetry. This Fe(0 0 1) surface state was first detected in tunneling spectroscopy by Stroscio et al. [26] and slightly later by Biedermann et al. [27]. Compared to the earlier work for which the peak in dI/dV was reported at +0.17 V [26], the peak is detected at a slightly lower energy in the measurement shown in Fig. 1b. Furthermore, the dI/dV feature is characterized by an almost Gaussian line shape in contrast to a weak peak on an exponential background reported in [26,27]. In the present study, it is found that the surface state peak can be observed between +0.13 and +0.20 V depending on the voltage dependence of the background. The peak is most pronounced for low background conditions, although in this case the apparent peak energy is lower than +0.17 V. Curve 2 represents the average of the dI/dV curves measured on the Mn islands. A clear peak is re-

solved at +0.45 V which gives strong evidence for the different chemical nature of the islands. The average of the dI/dV curves measured at the Fe(0 0 1) step edges shows that the surface state is completely quenched at monoatomic steps (curve 3). The dI/dV curves measured at island edges (not shown) show the same behavior. The observation that the high energy dI/dV background measured at the Fe(0 0 1) steps resembles the background observed on the islands better than the background observed on the terrace seems to imply that the Fe(0 0 1) step edges are completely wetted by Mn.

Fig. 1c and 1d shows maps of dI/dV at the voltage of the Fe(0 0 1) surface state (+0.16 V) and at a voltage which filters out the Mn peaks (i.e. +0.99 V) most clearly. The different electronic structure of the islands, steps and terraces is obvious from Fig. 1c. Line profiles over the steps (not shown) show that the surface state is quenched on a length scale of order 0.7 nm. This length scale is comparable to the broadening of the monoatomic steps in the constant current image of Fig. 1a which was measured at the same setpoint and with the same tip configuration. The spherical depressions in the dI/dV map of Fig. 1c are related to oxygen impurities on the Fe(0 0 1) surface. Their concentration is lower than 0.01 ML even some hours after deposition which is in contrast to the observations of Andrieu et al. who reported an oxidation rate of 0.03 ML/h for submonolayer Mn films on Fe(0 0 1) [8]. The averaged dI/dV curve representative of these impurities is also shown in Fig. 1b (curve 4) and reveals that at a single oxygen impurity the surface state dI/dV peak shifts ~0.03 V towards higher energy and has a 30% lower amplitude. The width of the oxygen-induced depressions in the dI/dV map is ~0.7 nm (full width at half maximum). The same order of peak shift and the same range of influence was recently reported for carbon impurities on V(0 0 1) [28]. This range is related to the lower resolution at the relatively high tunneling resistances used during STS [29] and must therefore be considered as an upper limit for the range of influence of the steps and the impurities on the electronic structure.

The dI/dV map at $V_s = +0.99$ V (Fig. 1d) shows the homogeneity of the Mn islands and the presence of Mn islands connected to the Fe(0 0 1) step. The island homogeneity also follows from a careful check of the single dI/dV curves obtained on the islands.

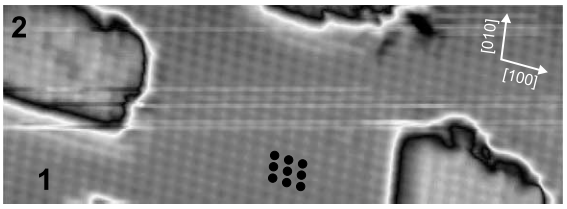

Fig. 2. Atomically resolved STM image obtained on Fe(0 0 1) covered with 0.2 ML Mn at 50 °C ($I = 3$ nA, $V_s = -5$ mV, 7.7×4.1 nm^2). A stepped grey scale has been used: the black–white range corresponds to 0.01 nm on the terrace (marked 1) and the island surface (marked 2). The black–white island borders are artifacts of the grey scale. The image has been averaged over 3×3 data points. A very weak p(1 × 1) lattice can be resolved of which the corrugation is less than ~2 pm. The black dots indicate the positions of the atoms. The close-packed directions are also shown.

An atomically resolved STM image of this sample is shown in Fig. 2. An undisturbed p(1 × 1) lattice with an extremely low corrugation (below ~2 pm) was always observed. In contrast to growth at higher temperatures, for growth at 50 °C no indications for Mn incorporation in the Fe(0 0 1) substrate layer were found. The close-packed directions of the Fe(0 0 1) lattice are indicated in this figure. Note that they do not make a perfect angle of 90° which is attributed to a thermal drift of typically ~0.3 nm/min shortly after deposition. In this paper, the STM images are not corrected for this drift.

In conclusion, from both the STM and STS results of the growth at 50 °C it is evident that no intermixing occurs at this temperature.

3.2. Submonolayer growth at elevated temperatures: surface alloying

3.2.1. Chemically resolved STM

An STM image of the Fe(0 0 1) surface after deposition of 0.37 ML Mn at a substrate temperature of 150 °C is shown in Fig. 3. The terraces and the islands (0.156 ± 0.005 nm high) now look completely different compared to the growth at 50 °C. At the low tunneling resistance

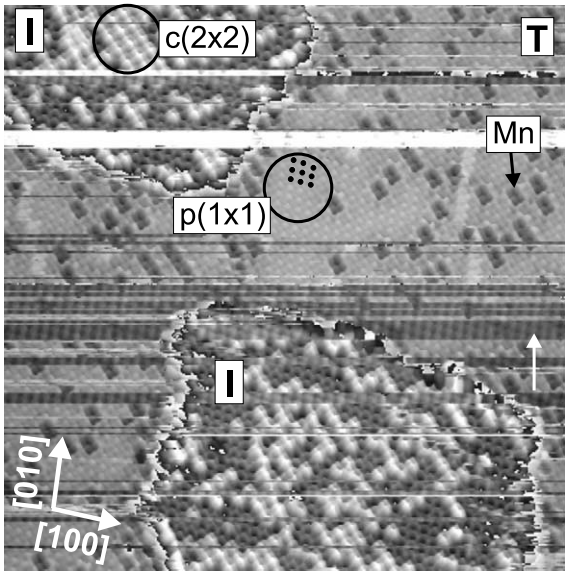

Fig. 3. STM image ($I = 1.4$ nA, $V_s = -5$ mV, 14.9×14.9 nm^2) of 0.37 ML Mn deposited on Fe(0 0 1) at 150 °C. A stepped grey scale has been used: the black–white range corresponds to 0.1 nm on the terrace (marked T) and the island surfaces (marked I). Chemical contrast is achieved: asymmetric depressions on the terrace are attributed to embedded Mn atoms and protrusions on the islands to incorporated Fe atoms. The protrusions on the islands are locally ordered in a $c(2 \times 2)$ structure. The area indicated by the white arrow does not show chemical contrast. The close-packed directions correspond to those indicated in Fig. 2.

used (i.e. $V_s = -5$ mV, $I = 1.4$ nA), it is generally not possible to keep a stable tip configuration while scanning over the islands. Consequently, tip changes are frequently observed in Fig. 3. No lateral shift occurs in the image after a tip change and the perpendicular shift is typically less than 0.1 nm. This indicates that only the tip apex atom is affected. Nevertheless, with particular tip conditions chemical contrast is achieved in the larger part of the image (e.g. no chemical contrast is observed in the area marked by the white arrow). The terrace is covered with asymmetric depressions which are 40 pm deep, while on the islands 20 pm high protrusions are observed. The strong dependence of the appearance of these features on tip conditions and the rather low stability of the tip configurations leading to these features makes it likely that the same mechanism is responsible for the chemical contrast as was reported by Schmid et al. in their studies on PtNi alloyed surfaces [30–32]. In these studies, a tip–sample interaction mediated by an unknown adsorbate on the tip was believed to lead to chemical contrast. The adsorbate (e.g. sulphur or oxygen impurity atoms) forms a precursor of a chemical bond, similar to a hydrogen bridge, more effectively with one type of surface atom than the other.

The depressions on the terrace are ascribed to single embedded Mn atoms and the protrusions on the islands to Fe atoms which have been released from the terrace after place exchange events. For this particular amount of Mn deposited at 150 °C (i.e. 0.37 ML), the concentration of Mn atoms in the terrace is 5%, while the concentration of Fe atoms in the islands is estimated to be 21%. 0.05 ML Mn of the 0.37 ML deposited, i.e. 14% of the Mn deposited, has therefore been place exchanged at this growth temperature. As can clearly be seen from this figure, the protrusions on the islands order locally in a $c(2 \times 2)$ structure which indicates the absence of a surface next-nearest neighbor repulsion as was reported for Cr/Fe(0 0 1) [18,19] and which is in agreement with theoretical predictions [17].

From STM images like Fig. 3 the concentration of Mn atoms embedded in the Fe(0 0 1) terrace and Fe atoms incorporated in the islands can be estimated as a function of growth temperature with reasonable accuracy. The results are shown in Table 1. The onset substrate deposition temperature for surface alloy formation is 100 °C, while submonolayer growth at 200 °C leads to islands which include large numbers of intermixed Fe atoms. At this growth temperature the step height of the island is found to be reduced to 0.148 ± 0.005 nm which is considered to be a consequence of the high Fe concentration in the islands. From the concentration of Fe atoms in the islands ($C^{\mathrm{exp}}_{\mathrm{Fe(i)}}$), the concentration of Mn atoms in the terrace ($C^{\mathrm{cal}}_{\mathrm{Mn(t)}}$) can be estimated under the assumption that the Mn atoms stay in the surface layer: i.e. $C^{\mathrm{cal}}_{\mathrm{Mn(t)}} = C^{\mathrm{exp}}_{\mathrm{Fe(i)}} \times$ coverage. The calculated concentrations are shown in the table and the good agreement with the observed Mn concentrations on the terrace ($C^{\mathrm{exp}}_{\mathrm{Mn(t)}}$) shows that the Mn atoms do indeed stay in the surface layer for the growth

Table 1
Amount of Mn deposited (coverage) as determined from histogram analysis on large terraces, concentration of Fe atoms in the islands $C^{exp}_{Fe(i)}$, and concentration of embedded Mn atoms in the Fe(0 0 1) terrace $C^{exp}_{Mn(t)}$ as a function of growth temperature T_{gr}. The concentration of embedded Mn atoms in the terrace $C^{cal}_{Mn(t)}$ is calculated under the assumption that all place exchanged Mn atoms are incorporated into the first substrate layer ($C^{cal}_{Mn(t)}$ = coverage × $C^{exp}_{Fe(i)}$). The fraction of deposited Mn atoms which exchange place with substrate Fe atoms ($C_{ex} = C^{exp}_{Mn(t)}$/coverage) is also shown

T_{gr} (°C)	Coverage [ML]	$C^{exp}_{Fe(i)}$ (at.%)	$C^{exp}_{Mn(t)}$ (at.%)	$C^{cal}_{Mn(t)}$ (at.%)	C_{ex} (at.%)
50 ± 10	0.17 ± 0.04	–	–	0	0
100 ± 20	0.38 ± 0.04	18 ± 2	4 ± 2	7 ± 1	11 ± 6
150 ± 30	0.37 ± 0.04	21 ± 2	5 ± 2	8 ± 1	14 ± 6
175 ± 30	0.51 ± 0.04	17 ± 5	12 ± 2	9 ± 3	24 ± 4
200 ± 30	0.36 ± 0.04	60 ± 5	20 ± 4	22 ± 3	56 ± 13

temperatures studied. For Cr deposited on Fe(0 0 1) it was reported that for growth at 300 °C and coverages between 0.2 and 1 ML only ~0.1 ML Cr atoms were found on the surface while for growth at lower temperatures the degree of intermixing was reduced [18].

For STM experiments performed at room temperature, the atomic processes leading to the surface alloy are too rapid to be imaged directly. The low density of steps on Fe(0 0 1) whisker surfaces and the large calculated energy gain for place exchange (0.65 eV for Mn compared to 0.57 eV for Cr [17]) makes it very likely that Mn atoms are incorporated in the Fe(0 0 1) surface without moving to steps first. The incorporation may involve either a direct place exchange mechanism [33] or annihilation of vacancies which were originally formed at kinks or steps. In the latter case, the diffusion of the vacancies from the kink or step to the terrace must be faster than the diffusion of the Mn adatoms to the steps. If the adatoms diffuse faster, the vacancies are annihilated by Mn adatoms close to step edges and consequently the highest concentration of incorporated Mn atoms will be found here. This was shown to be the case for e.g. Mn on Cu(0 0 1) [34], Pb on Cu(1 1 1) [35] and Pb on Cu(0 0 1) [36]. In the present study, the distribution of incorporated Mn atoms is homogeneous on the terrace and there is no evidence for higher Mn concentrations around islands and substrate step edges even for growth at 100 °C. However, the observation that pure Mn islands form at 50 °C while the onset for Mn incorporation is 100 °C seems to suggest that diffusion dominates over place exchange for growth temperatures below 100 °C. Therefore, it cannot be excluded that Mn adatoms diffuse to islands first and place exchange with substrate atoms at step edges and kink sites [34]. Subsequent step fluctuations and vacancy-mediated diffusion may lead to a more homogeneous distribution of the Fe atoms in the Mn islands and of the embedded Mn atoms in the Fe(0 0 1) substrate [34].

From Table 1 the fraction of place exchanged Mn atoms (C_{ex}) can be estimated by dividing the observed number of Mn atoms embedded in the terrace ($C^{exp}_{Mn(t)}$) by the amount which had been deposited (coverage). This fraction is shown as a function of temperature both in the last row of the table and in Fig. 4. It clearly shows that for the coverage regime studied, the fraction of place exchanged Mn atoms increases as a function of temperature. However, the place exchanged frac-

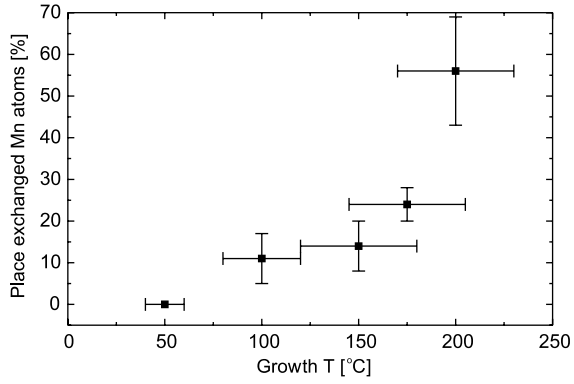

Fig. 4. Concentration of deposited Mn atoms which have place exchanged with substrate Fe atoms (C_{ex}) as a function of growth temperature.

tion cannot be fitted by a simple activation law (i.e. $C_{ex} \sim \exp(-E_a/kT)$, with E_a an activation energy) showing the complexity of the processes involved. It might be wondered if for growth at even higher temperatures the fraction of place exchanged Mn atoms increases to 100% and if Mn atoms eventually do dissolve into the bulk. However, our setup does not allow growth at higher temperatures and post-annealing is believed to lead to different results.

3.2.2. STS on alloyed surface layer

In order to study the electronic structure of the Mn atoms embedded in the terrace and the Fe atoms incorporated in the islands, STS measurements were performed. As shown in Fig. 5 the dI/dV curves measured on the terrace protrusions (curve 2), i.e. incorporated Mn atoms, do not differ much from those obtained on the clean Fe(0 0 1) terrace (curve 1). Both curves, which are averages of typically 10 single dI/dV curves, show a peak at +0.17 V, although this peak has a 25% lower intensity on the Mn atoms. The insets in this figure show the topographic image taken at the setpoint of spectroscopy (top left) and the corresponding dI/dV map at the surface state energy +0.17 V (bottom right). The minima in this dI/dV map are correlated with the protrusions in the topographic image.

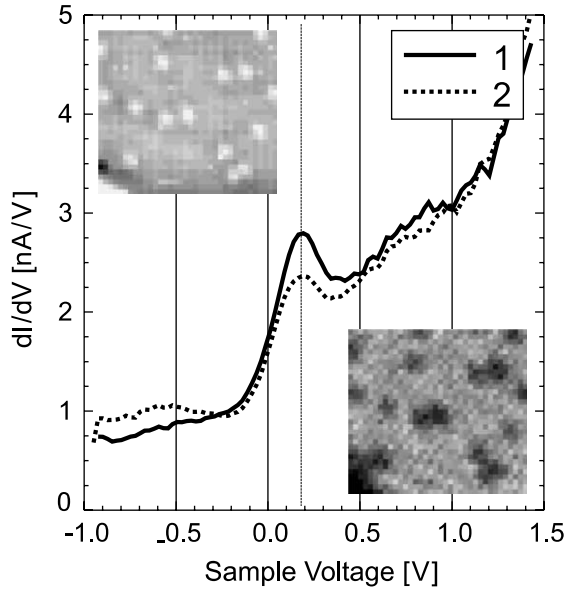

Fig. 5. STS measurement on isolated Mn atoms in the Fe(0 0 1) terrace ($I = 0.5$ nA and $V_s = -0.5$ V). Curves 1 and 2 are representative of dI/dV curves measured on the clean terrace and Mn atoms, respectively. The insets show the corresponding topographic image (top left: scan size is 4.8×4.4 nm^2, with this tip condition the Mn atoms are visible as 5 pm high protrusions) and the dI/dV map at $V_s = 0.17$ V (bottom right).

The topographic image shows that at the STS setpoint the Mn atoms have an apparent height of 5 pm. Since the Mn atoms can be imaged either as protrusions or depressions depending on tunneling conditions, it seems reasonable to ascribe this apparent height to electronic effects and/or tip–sample interaction effects rather than to a real geometric effect. However, care has to be taken since it is not trivial to distinguish between geometric and electronic effects in STM images (e.g. see [37]). It should also be realized that the atomic radius of Mn is 9 pm larger than of Fe [38] and buckling effects cannot be excluded [12,13] (although for the antiferromagnetically coupled substrate Mn atom the interlayer distance is always lowered in the calculations, 3 pm in [12] and 0.3 pm in [13]). Nevertheless, if these effects are ignored, the apparent height of 5 pm, thus, implies that the tip retracts 5 pm when over the Mn atom. This retraction leads to a 10% drop in the tunneling conductance, $\exp(-2\kappa\Delta) = 0.90$ (with $\kappa = 1 \times 10^{10}\text{m}^{-1}$ and tip retraction Δ of 5 pm) [29]. The reduction of 25% on top of the Mn atom can therefore only be partially ascribed to a larger tip–sample distance.

The calculations of Papanikolaou et al. show a 30% reduction in the LDOS 0.55 nm above the surface when a surface Fe atom is replaced by a Mn atom [20]. According to these calculations this peak arises from the pure Fe surface: it was shown that its relative weight (e.g. compared to the additional peak observed in the calculations for Cr impurities) increases for larger tip–sample distances due to the larger area that is probed by the tip. This prediction seems to be in qualitative agreement with our experimental results taking into account the different tip–sample distances for dI/dV measurements on Fe(0 0 1) and on surface substitutional Mn sites. However, the absolute tip–sample distances in the measurements are not

known which makes a quantitative comparison impossible.

The dI/dV curve measured on the Mn atom also shows a higher dI/dV signal below $V_s = -0.2$ V compared to the clean Fe(0 0 1) curve. This feature might be related to the weak and broad peak at -0.7 eV found in the calculated minority band LDOS in the vacuum (at 0.55 nm above the surface) [20]. However, the experimental feature is too weak to base any strong claims on it. Observation of occupied sample LDOS peaks is not very favorable due to the higher tunneling barrier experienced for tunneling from these states (e.g. the tunneling probability is reduced by a factor 0.2 for sample states 0.5 eV below the Fermi level at 1 nm above the surface [26]). Nevertheless, this decay is already included in the calculated vacuum LDOS. Furthermore, unlike for the other impurities, the calculations for Mn predict a strong peak around $+1$ eV in the majority band. This peak was, however, never observed in the experiments (see e.g. Fig. 5).

Results of STS measurements performed on the intermixed islands are shown in Fig. 6. dI/dV curves were obtained on the surface area shown in the atomically resolved STM image of Fig. 6a (same island as imaged in Fig. 3). Based upon the dI/dV map at $V_s = +0.99$ V (Fig. 6b) three kinds of dI/dV spectra can be distinguished. Averages of these spectra (typically obtained from $\sim$100 curves) are shown in Fig. 6c. Curve 1 is measured on the clean Fe(0 0 1) terrace and shows the Fe(0 0 1) surface state as a peak at $+0.20$ eV. Comparing the topographic image (Fig. 6a), the dI/dV map (Fig. 6b) and the dI/dV curves (Fig. 6c) shows that curve 2 (with low dI/dV at $+1$ V) is

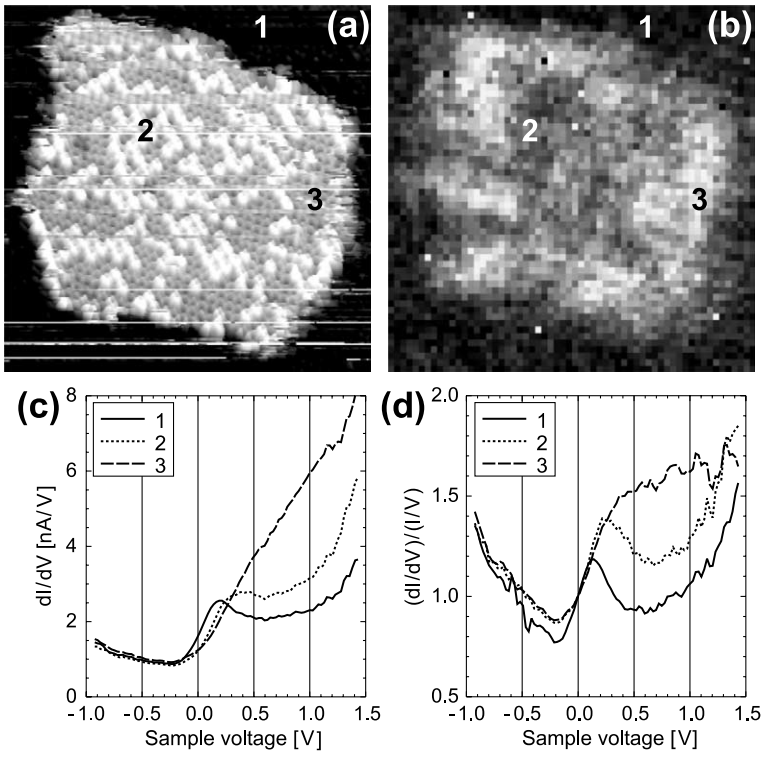

Fig. 6. STS measurement on Fe(0 0 1) covered with 0.37 ML Mn deposited at 150 °C. (a) Topographic image ($I = 0.5$ nA, $V_s = -5$ mV, 4.8×4.4 nm^2). At this area dI/dV is measured at setpoints $I = 0.5$ nA, $V_s = -0.54$ V. (b) dI/dV map at $V_s = +0.99$ V. (c) Three different types of dI/dV curves (curves are averaged) are obtained: curve 1 is measured on the Fe(0 0 1) terrace, curve 2 on the local c(2 × 2) MnFe surface alloy and curve 3 on the p(1 × 1) Mn areas on the islands. (d) dI/dV curves of (c) normalized by I/V.

correlated with the protrusions, and curve 3 (with high dI/dV at +1 V) with the topographic dark p(1 × 1) areas. Curve 2 shows a peak at +0.35 eV, while no peaks are visible in curve 3. Nevertheless, it is clear that at positive bias voltages there is an additional contribution to dI/dV curve 3 on top of the exponential background (see also Fig. 8). As discussed previously, the protrusions on the islands were identified as Fe atoms which have been released from the Fe(0 0 1) terrace after place exchange events and intermixed with Mn islands. Curve 2 is therefore representative of a c(2 × 2)-like clustering of Mn and Fe atoms and curve 3 for a pure Mn adlayer on Fe(0 0 1).

The absence of a peak on the pure Mn part of the island in the dI/dV measurement of Fig. 6c might seem conflicting with the observation of a peak at +0.45 V in the measurement of Fig. 1b. A different electronic structure cannot be excluded due to the possibility of the Mn atoms being differently coordinated, i.e. four (zero) Fe (Mn) nearest neighbors for growth at 50 °C and four or less (zero or more) Fe (Mn) nearest neighbors for growth at 150 °C. Growth at different temperatures may also stabilize different magnetic unit cells with inequivalent electronic structures [15]. Nevertheless, the effect can be perfectly explained by an intrinsic artifact of STS measurements: the presence of a voltage dependent background.

In the dI/dV curve measured on the clean Fe(0 0 1) surface shown in Fig. 1b almost no exponential background is visible on the high-energy side of the peak and consequently, the peak exhibits a Gaussian-like shape. In Fig. 6c, however, the clean Fe(0 0 1) dI/dV curve has a much larger exponential background on the high-energy side of the peak. The background is clearly related with the tip configuration: voltage pulses (up to ±10 V) almost always lead to a change of this background. In Fig. 7 two extreme cases are shown: the left dI/dV curve shows a Gaussian-like shape with a weak exponential background, while for the right curve this background is high on the positive energy side. To categorize the different peak shapes observed with different tip conditions, a parameter which characterizes the amount of background is defined. A possible parameter, which has the advantage that it is easily obtained

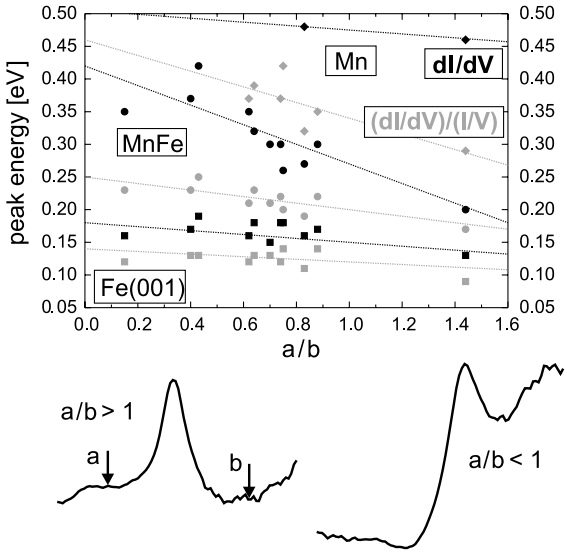

Fig. 7. Peak energies observed in STS as a function of background. The background parameter a/b is defined as the ratio between the local minimum dI/dV on the low-energy side of the Fe(0 0 1) surface state peak (a) and the local minimum dI/dV on the high-energy side (b). Therefore, a low (high) background on the high-energy side corresponds to high (low) a/b. The dI/dV peak energies obtained on the clean Fe(0 0 1) terrace, MnFe c(2 × 2) alloyed areas, and Mn p(1 × 1) areas are shown as black squares, circles and diamonds, respectively. Grey symbols are used for the corresponding peak energies in $(dI/dV)/(I/V)$. The data points are fitted to linear functions to guide the eye.

from experimental data, is the ratio a/b between the (local) minimum in dI/dV on the low-energy side of the clean Fe(0 0 1) peak a and the (local) minimum in dI/dV on the high-energy side b. a and b are indicated in Fig. 7. With this definition, Gaussian peak shapes correspond to $a/b \sim 1$, while dI/dV curves which exhibit a high exponential background on the high-energy side correspond to $a/b < 1$. In Fig. 7 the dI/dV peak energies obtained on the clean Fe(0 0 1) surface are plotted as a function of this parameter (black squares). The apparent peak energy varies between +0.13 and +0.20 V with a clear trend that a low (high) peak energy is found if the high energy background is absent (present).

Normalizing dI/dV by I/V does not help too much (grey squares in Fig. 7): now the peak energy shifts between +0.09 and +0.15 V with the same

trend. The normalized curves obtained on the Mn islands grown at 150 °C are shown in Fig. 6d. It shows that peaks at high energies which are heavily distorted by the background in dI/dV are more pronounced in $(dI/dV)/(I/V)$ although for even higher energies the peak is disturbed by the background in $(dI/dV)/(I/V)$ as well (curve 3 in Fig. 6d). Therefore, a tip configuration which suppresses this background is most desirable to resolve the high-energy peaks in dI/dV (and $(dI/dV)/(I/V)$). This is the case for the measurement shown in Fig. 1b.

The peak energies observed on the MnFe alloyed island areas (circles) and the pure p(1 × 1) Mn island areas (diamonds) are also shown in Fig. 7 as a function of the background parameter a/b. Peak energies in dI/dV and $(dI/dV)/(I/V)$ are indicated by black and grey symbols, respectively. As a function of background parameter a/b, dI/dV peak energies between +0.20 and +0.43 V can be found for the alloyed areas and between +0.45 and +0.50 V for the pure Mn islands (although these peaks are only observed for quite high a/b for which the background is suppressed which explains why there are only two data points for the dI/dV peaks measured on pure Mn islands in Fig. 7). The peak energies in $(dI/dV)/(I/V)$ vary between +0.17 and +0.25 V for the c(2 × 2) MnFe areas, and between +0.29 and +0.42 V for the pure Mn islands. Obviously, low (high) peak energies are found for low (high) background, and peak energies in $(dI/dV)/(I/V)$ are always lower than those in dI/dV. The fitted lines in Fig. 7 are intended as a guide to the eye.

Ukraintsev has shown that neither dI/dV nor $(dI/dV)/(I/V)$ reflect the real sample LDOS even within a simplified one-dimensional WKB approach [39]. Both quantities represent the LDOS convoluted with a tunneling probability function which also contains the tip density of states at the Fermi level for positive bias voltages. Ukraintsev proposed to normalize dI/dV with its fitted tunneling probability function: this deconvolution technique is considered to lead to the best recovery of the sample LDOS, at least within the one-dimensional WKB approximation of tunneling. However, the deconvolution technique proposed by Ukraintsev is not very practical since it requires dI/dV data over a large voltage range to allow for an accurate fitting of the background. Such a large voltage range is usually not available. Stroscio et al. deduced the surface state energy of clean Fe(0 0 1), i.e. +0.17 V, by a fit of a Gaussian function plus quadratic background to the dI/dV data [26] which can be considered as a simple approximation to the Ukraintsev approach. We verified that normalizing the dI/dV curve measured on the clean Fe(0 0 1) shown in Fig. 6 (and many other curves) by a quadratic function shifts the Fe(0 0 1) surface state from +0.20 to +0.17 V as well. This gives a strong motivation to use this method for LDOS recovery also for the dI/dV curves measured on the pure Mn p(1 × 1) island areas and the MnFe c(2 × 2) alloyed areas.

Fig. 8 shows the results of this deconvolution. In Fig. 8a the dI/dV curve measured on the pure Mn island (see Fig. 1b) and two quadratic functions fitted to the high energy background of this curve are shown. Due to the small voltage range used (up to +1.5 V) the fits are not very accurate and the two fits shown in Fig. 8a reflect two extremes. However, the two normalized curves are almost equal and both show a peak at +0.34 V. This gives an indication that the fits to the tunneling probability do not need to be perfect to give a reasonable estimate of the surface state energy. Also shown in Fig. 8a is a dI/dV curve measured on pure Mn which shows a strong background in which no peak can be resolved (see Fig. 6c). Normalizing this curve by its quadratic fit (which can only be a very rough estimate of the real tunneling probability function), leads to a curve showing a peak at +0.37 V.

In Fig. 8b two dI/dV curves measured on the MnFe c(2 × 2) alloyed areas are shown (one curve is the curve of Fig. 6c). Normalizing these curves by quadratic functions fitted to their high energy backgrounds recovers peaks at +0.26 V for both cases. Therefore, although dI/dV curves need to be measured over large voltage ranges to allow for a more accurate fitting of the background, our results imply that even imperfect fits to quadratic functions lead to a relatively accurate recovery of the real surface state energies. In the present study, we estimate the surface state energies of the p(1 × 1) Mn islands and the c(2 × 2) MnFe alloy

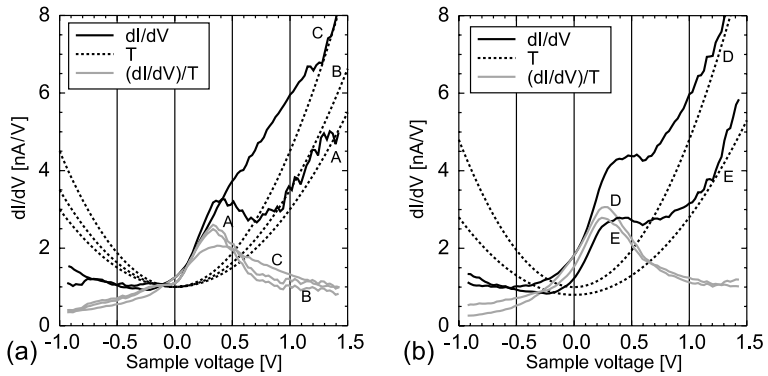

Fig. 8. dI/dV curves (black drawn) measured on pure Mn p(1 × 1) island areas (a) and MnFe c(2 × 2) alloyed areas (b). In both (a) and (b) two dI/dV curves with different backgrounds due to different tip configurations (see text) are shown. The background on the high-energy side of these curves have been fitted by quadratic functions T (A, B, C, D and E; black dotted curves). dI/dV curves with different backgrounds show the same peak energy (within 0.05 V) in $(dI/dV)/T$ (grey drawn curves). In (a) the dI/dV curve showing a peak was normalized using two separate backgrounds (A and B). The corresponding dI/dV curves are almost identical showing that the fit of T to the background in dI/dV does not have to be extremely accurate.

to be $+0.35 \pm 0.05$ V and $+0.25 \pm 0.05$ V, respectively.

The different backgrounds appearing under different tip configurations may be a result of the apex having either metallic (e.g. W, Fe or Mn atom) or non-metallic (e.g. O) character. Measurements of apparent barrier heights showed that with tips leading to small backgrounds high apparent barrier heights are found (~5 eV), while with tips showing an extreme high background low apparent barrier heights are found (~3 eV). Both kind of tips image monoatomic steps with the same sharpness and tip changes mostly lead to tip displacements of less than 0.1 nm. Both observations imply that the tip changes only involve an exchange of the apex atom. Electronegative adsorbates like oxygen are known to increase work functions on tungsten surfaces (see e.g. [40,41]) which implies that the absence of background in dI/dV might be related to slightly contaminated tip configurations. Furthermore, atomically sharp tungsten tips are expected to have smaller work functions than close-packed surfaces [42] which might explain why apparent barrier heights as low as ~3 eV are measured. Moreover, it is not unlikely that the lower conductivity of non-metallic tips leads to smaller tip–sample distances at a given setpoint: the tunneling probability function within a one-dimensional WKB approximation (see e.g. [39]) shows that at smaller tip–sample distances the voltage dependence of the tunneling probability function is reduced. The influence of different tip configurations on the appearance of the voltage dependent background in dI/dV curves can now be qualitatively understood.

4. Conclusion

STM measurements showed that Mn atoms become incorporated in the Fe(0 0 1) surface for submonolayer growth at temperatures above 100 °C. From images showing chemical contrast the fraction of Mn atoms that have undergone place exchanges with Fe substrate atoms was deduced as a function of growth temperature. A local c(2 × 2) structure was observed on the islands which was interpreted as an ordered MnFe alloy. For the growth temperatures studied (up to 200 °C) the Mn atoms were found to stay in the surface layer. STS measurements did not reveal a double peak structure in the dI/dV spectra on the single Mn impurities in contrast to Cr/Fe(0 0 1). The influence of a tip dependent background on the apparent surface state energies in dI/dV and $(dI/dV)/(I/V)$ was discussed and carefully analyzed. By normalizing the dI/dV curves by fitted quadratic backgrounds the surface state energies

were recovered. Pure p(1 × 1) Mn islands were found to show a surface state around +0.35 V, while the c(2 × 2) MnFe alloyed areas on the islands showed a surface state around +0.25 V.

Acknowledgements

This work was supported by the Stichting voor Fundamenteel Onderzoek der Materie (FOM), which is financially supported by the Nederlandse Organisatie voor Wetenschappelijk Onderzoek (NWO), and the European Growth project MAGNETUDE. T.Y. acknowledges Gakushuin University (Tokyo, Japan) for a travel grant. We gratefully thank B. Heinrich (Simon Fraser University, Burnaby, Canada) for supplying the Fe whiskers.

References

[1] D.A. Tulchinsky, J. Unguris, R.J. Celotta, J. Magn. Magn. Mater. 212 (2000) 912.
[2] D.T. Pierce, A.D. Davies, J.A. Stroscio, D.A. Tulchinsky, J. Unguris, R.J. Celotta, J. Magn. Magn. Mater. 222 (2000) 13.
[3] S.T. Purcell, M.T. Johnson, N.W. McGee, R. Coehoorn, W. Hoving, Phys. Rev. B 45 (1992) 13064.
[4] S.K. Kim, Y. Tian, M. Montesano, F. Jona, P.M. Marcus, Phys. Rev. B 54 (1996) 5081.
[5] R. Pfandzelter, T. Igel, H. Winter, Surf. Sci. 389 (1997) 317.
[6] S. Andrieu, M. Finazzi, Ph. Bauer, H. Fischer, P. Lefevre, A. Traverse, K. Hricovini, G. Krill, M. Piecuch, Phys. Rev. B 57 (1998) 1985.
[7] S. Andrieu, M. Finazzi, F. Yubero, H. Fischer, P. Arcade, F. Chevrier, K. Hricovini, G. Krill, M. Piecuch, J. Magn. Magn. Mater. 165 (1997) 191.
[8] S. Andrieu, E. Foy, H. Fischer, M. Alnot, F. Chevrier, G. Krill, M. Piecuch, Phys. Rev. B 58 (1998) 8210.
[9] Ch. Roth, Th. Kleeman, F.U. Hillebrecht, E. Kisker, Phys. Rev. B 52 (1995) R15691.
[10] O. Rader, W. Gudat, D. Schmitz, C. Carbone, W. Eberhardt, Phys. Rev. B 56 (1997) 5053.
[11] J. Dresselhaus, D. Spanke, F.U. Hillebrecht, E. Kisker, G. van der Laan, J.B. Goedkoop, N.B. Brookes, Phys. Rev. B 56 (1997) 5461.
[12] R. Wu, A.J. Freeman, Phys. Rev. B 51 (1995) 17131.
[13] S. Handschuh, S. Blügel, Solid State Commun. 105 (1998) 633.
[14] O. Elmouhssine, M. Freyss, P. Krüger, J.C. Parlebas, C. Demangeat, J. Khalifeh, A. Vega, A. Mokrani, Phys. Rev. B 55 (1997) R7410.
[15] S. Heinze, Ph.D. Thesis, University of Hamburg, 2000.
[16] M. Taguchi, O. Elmouhsinne, C. Demangeat, J.C. Parlebas, Phys. Rev. B 60 (1999) 6273.
[17] B. Nonas, K. Wildberger, R. Zeller, P.H. Dederichs, Phys. Rev. Lett. 80 (1998) 4574.
[18] A. Davies, J.A. Stroscio, D.T. Pierce, R.J. Celotta, Phys. Rev. Lett. 76 (1996) 4175.
[19] A. Davies, J.A. Stroscio, D.T. Pierce, J. Unguris, R.J. Celotta, J. Magn. Magn. Mater. 165 (1996) 82.
[20] N. Papanikolaou, B. Nonas, S. Heinze, R. Zeller, P.H. Dederichs, Phys. Rev. B 62 (2000) 11118.
[21] T. Igel, R. Pfandzelter, H. Winter, Surf. Sci. 405 (1998) 182.
[22] T.G. Walker, H. Hopster, Phys. Rev. B 48 (1993) 3563.
[23] S.T. Purcell, A.S. Arrott, B. Heinrich, J. Vac. Sci. Technol. B 6 (1988) 794.
[24] G. de Raad, P. Koenraad, J.H. Wolter, J. Vac. Sci. Technol. B 17 (1999) 1946.
[25] H. Röder, R. Schuster, H. Brune, K. Kern, Phys. Rev. Lett. 71 (1993) 2086.
[26] J.A. Stroscio, D.T. Pierce, A. Davies, R.J. Celotta, M. Weinert, Phys. Rev. Lett. 75 (1995) 2960.
[27] A. Biedermann, O. Genser, W. Hebenstreit, M. Schmid, J. Redinger, R. Podloucky, P. Varga, Phys. Rev. Lett. 76 (1996) 4179.
[28] M.M.J. Bischoff, Ch. Konvicka, A.J. Quinn, M. Schmid, J. Redinger, R. Podloucky, P. Varga, H. van Kempen, Phys. Rev. Lett. 86 (2001) 2396.
[29] J. Tersoff, D.R. Hamann, Phys. Rev. B 31 (1985) 805.
[30] M. Schmid, H. Stadler, P. Varga, Phys. Rev. Lett. 70 (1993) 1441.
[31] M. Schmid, A. Biedermann, P. Varga, Surf. Sci. Lett. 294 (1993) L952.
[32] P. Varga, M. Schmid, Appl. Surf. Sci. 141 (1999) 287.
[33] G.L. Kellogg, P.J. Feibelman, Phys. Rev. Lett. 64 (1990) 3143;
P.J. Feibelman, Phys. Rev. Lett. 65 (1990) 729.
[34] T. Flores, S. Junghans, M. Wuttig, Surf. Sci. 371 (1997) 14.
[35] C. Nagl, O. Haller, E. Platzgummer, M. Schmid, P. Varga, Surf. Sci. 321 (1994) 237.
[36] C. Nagl, E. Platzgummer, O. Haller, M. Schmid, P. Varga, Surf. Sci. 331–333 (1995) 831.
[37] D. Wortmann, S. Heinze, G. Bihlmayer, S. Blügel, Phys. Rev. B 62 (2000) 2862.
[38] C.L. Smithells, E.D. Brandes, Metals Reference Book, Butterworths, London, 1978.
[39] V.A. Ukraintsev, Phys. Rev. B 53 (1996) 11176.
[40] J.E. Whitten, R. Gomer, Surf. Sci. 409 (1998) 16.
[41] H. Kawano, T. Takahashi, Y. Tagashira, H. Mine, M. Moriyama, Appl. Surf. Sci. 146 (1999) 105.
[42] W.A. Hofer, J. Redinger, Surf. Sci. 447 (2000) 51.